Correlations in trapped Plasma

François Anderegg
University of California San Diego, Physics Dept. 0319,
La Jolla CA 92093, USA
fanderegg@UCSD.edu

This chapter describes the effects of correlations on trapped plasma. When the potential energy between neighboring ions is larger than the thermal energy, the internal structure of trapped plasma changes, from plasma to liquid to Coulomb crystal. These Coulomb crystals are similar to solid state one but the inner particle spacing is of the order of 10μm, significantly larger than solid state material. The structure of these Coulomb crystal is obtained not from x-ray scattering but from Bragg scattering of UV light ($\sim$ 300nm). Correlations not only change equilibrium properties of a plasma but also dynamical properties, in particular this chapter will describe the dramatic increase of the collision rate in the presence of correlations.

1. Introduction

The thermodynamic state of a one component plasma is determined by its shape, size, and coupling parameter Γ :

$$\Gamma = \frac{1}{4\pi\epsilon_0}\frac{q^2}{a_{ws}k_BT} \tag{1}$$

where a_{ws} is the Wigner-Seitz radius:

$$a_{ws} \equiv \left(\frac{3}{4\pi n}\right)^{\frac{1}{3}} \tag{2}$$

a_{ws} is the radius of a sphere whose volume equal the volume occupied by one charged particle in a plasma of density n. The coupling parameter Γ represents the ratio of the potential energy between neighboring charged

particle and the thermal energy. When $\Gamma > 1$ a one component plasma is strongly coupled. Large value of coupling parameter can be achieved with high density n, or large charge per particle q, or low temperature T.

Strongly coupled one component plasmas are believed to exist in dense astrophysical objects such as giant planets interior (T ∼1eV, $n \sim 10^{24}\text{cm}^{-3}, q =$ e, resulting in $\Gamma \sim 10$), white dwarf stars (T ∼100eV, $n \sim 10^{30}\text{cm}^{-3}, q =$ e, resulting in $\Gamma \sim 10$).[1] Strongly coupled plasmas also exist in less dense objects if the charge per particle is large, such as dust grain in a dusty plasma[2] (T^{dust} ∼1eV, $n \sim 1\text{cm}^{-3}$, $q = 10^4$ e, resulting in $\Gamma \sim 10$), or if the temperature is low enough in laser cooled trapped ion plasma ($T \sim 10^{-5}$eV, $n \sim 10^{7}\text{cm}^{-3}, q = e$, resulting in $\Gamma \sim 10$). One sees that these vastly different physical systems, can all have a coupling parameter $\Gamma \sim 10$. Therefore astrophysical effects depending on Γ can be studied with laser cooled trapped ion, as will be described in section 3 of this chapter.

For coupling parameter $\Gamma \ll 1$ trapped ions are in a "plasma state", for $\Gamma > 1$ trapped ions are in a liquid state and for $\Gamma \gtrsim 172$. trapped ions are in a solid state called a Coulomb crystal.

2. Effect of Correlations on Equilibrium properties

In a trapped ion plasma consisting of many particles ($N \gg 1$), even when the correlation parameter Γ is large, the mean electric potential is large compared to the potential energy between neighboring ions.

$$e\phi \gg \frac{e^2}{4\pi\epsilon_0\, a_{ws}} \tag{3}$$

The mean electric potential determines the equilibrium shape of the plasma in the trap. The plasma shape remains essentially unchanged by the presence of correlation, the correlations only change the internal structure of the plasma, not its shape.

In the absence of correlation, the "one" particle distribution function is a Boltzman distribution.

$$f(r,v) = C\exp\left(\frac{-1}{k_B T}\ [H + \omega P_\theta]\right) \tag{4}$$

where the Hamiltonian H is:

$$H = \frac{mv^2}{2} + e(\phi_T + \phi_p) \tag{5}$$

ϕ_T is the trap potential and ϕ_p is the plasma potential which is determined by Poisson's equation:

$$\nabla^2\phi_p = \frac{-en}{\epsilon_0} \tag{6}$$

and the canonical angular momentum P_θ in a uniform magnetic field in the z-direction is:

$$P_\theta = mv_\theta r + \frac{eB}{2}r^2 \tag{7}$$

In contrast, when correlations are present, the N particle distribution is a Gibbs distribution:

$$f(r_1, v_1, r_2, v_2 \ ... \ r_N, v_N) = C \exp\left(\frac{-1}{k_B T} \ [H^{(N)} + \omega P_\theta^{(N)}]\right) \tag{8}$$

where the N particle Hamiltonian is:

$$H^{(N)} = \sum_{i=1}^{N} \frac{mv_i^2}{2} + e\left(\phi_T(r_i) + \sum_{j>i}\phi_{ij}\right) \tag{9}$$

where ϕ_T is the trap potential and ϕ_{ij} the interaction potential:

$$\phi_{ij} = \frac{e^2}{4\pi\epsilon_0|r_i - r_j|} \ + \text{"image charge"} \tag{10}$$

ϕ_{ij} is a Green function when the image charges are included.[3] In this chapter we assume that the image charge contribution is negligible, that is the plasma is far from the wall of the trap.
The N particle canonical angular momentum is:

$$P_\theta^{(N)} = \sum_{i=1}^{N}\left(mv_{\theta i}r_i + \frac{eB}{2}r_i^2\right) \tag{11}$$

and the N particles distribution becomes:

$$\begin{aligned} f(r_1, v_1, r_2, v_2 \ ... \ r_N, v_N) &= C \exp\left(\sum_{i=1}^{N}\frac{m}{2k_B T}\left[v_i + \omega r_i\hat{\theta}_i\right]\right) \\ &+ \ \tilde{C}\exp\left(-\sum_{i=1}^{N}\frac{1}{k_B T}\left[\frac{1}{2}\sum_{i\neq j}\frac{e^2}{4\pi\epsilon_0|r_i - r_j|} + e\phi_T\right]\right) \end{aligned} \tag{12}$$

Useful quantities to be considered are the reduced distribution; for example the spatial distributions are obtained by integrating over velocities, and the N-particle spatial distribution is:

$$\rho^{(N)}(r_1, r_2, ...r_M) = \int d^3r_{M+1}...d^3r_N \ \ f(r_1, ...r_N) \tag{13}$$

The density is simply the first reduced distribution:

$$n(r) = N\rho^{(1)}(r) \tag{14}$$

The two particles distribution is:

$$\rho^{(2)}(r_1, r_2) = \rho^{(1)}(r_1)\ \rho^{(1)}(r_2)\ [1 + g(r_1, r_2)] \tag{15}$$

where $g(r_1, r_2)$ represents the two body spatial correlations which measure the extra probability beyond what would be expected of a completely random distribution of finding particle at r_1 and r_2.

Since Coulomb interaction is a binary interaction, only $n(r)$, T and $\rho^{(2)}(r_1, r_2)$ are necessary to describe thermodynamic functions. No higher order term are necessary. Figure 1 shows the correlation function $g(r_1, r_2)$ for a one component plasma for various value of correlation parameter.[4]

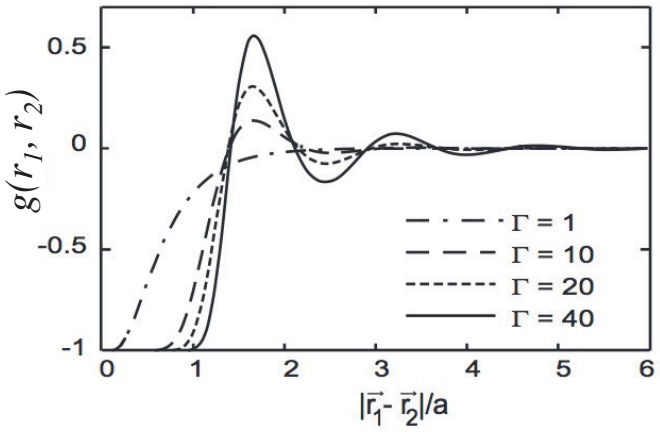

Fig. 1. Correlation function for one component plasma.

In the absence of correlation, the correlation function is equal to zero at large distance, and goes to minus one at short distance reflecting the effect of Debye shielding. As the correlation parameter Γ increases, $g(r_1, r_2)$ increases at a distance of about 1.7 Wigner-Seitz radius; for distance smaller than one Wigner-Seitz radius $g(r_1, r_2)$ decreases, indicating that short range order is appearing in the system. These oscillations are evidence of the beginning of a crystal lattice.

2.1. *Correlation with Small Plasmas*

Early numerical simulations[5] solved the following equations for $N = 400$ ions:

$$\begin{aligned}
\frac{dx_i}{dt} &= \frac{E_i}{B} \times \hat{z} + U_i \hat{z} \\
\frac{dU_i}{dt} &= \frac{mE_i}{e} \hat{z} \\
E_i &= \frac{-\partial \Phi}{\partial x_i} \\
e\Phi(x_i, ..., x_N) &= \sum_{i>j} \frac{e^2}{4\pi\epsilon_0 |x_i - x_j|} + \sum_i \frac{1}{2} m\omega_z^2 \left(z_i^2 - \frac{\rho_i^2}{2} \right)
\end{aligned} \tag{16}$$

where one can see the potential Φ is the same as the first term of equation 10 and that the trap potential is the standard quadratic potential of a Penning trap. These simulations show that for small plasmas, boundary effect dominates the geometry and inside the plasma ions are organized in a concentric shell structure.

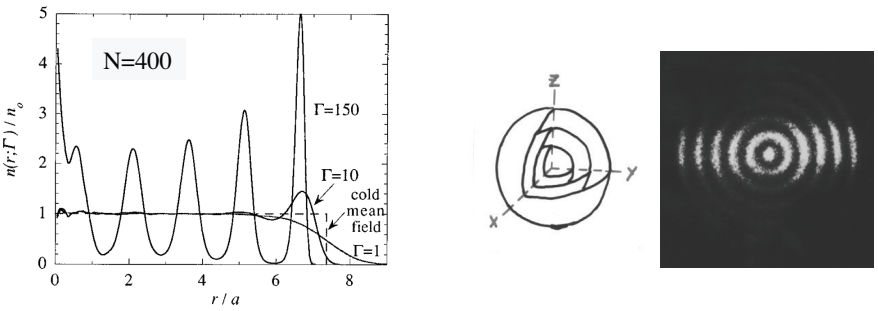

Fig. 2. a) Density as a function of spherical radius b) Observation of shell structure in Penning trap.

The results of these simulations are shown on figure 2a, at low Γ the normalized spatial distribution is uniform, in contrast for large Γ sharp "onion-like shell" are predicted. Figure 2b is a measurement of such structure on a cloud of beryllium ions.[6] The number of shells observed depend on the number of ions N, with $N = 20$, 1 shell is observed and with $N = 15,000$, 16 shells are observed.

2.2. *Correlation with Large Plasmas*

The influence of the surface is limited for large plasma and their interior is comparable to an infinite size plasma. The lowest energy state for a Coulomb crystalline structure is a Body Center Cubic (bcc) structure followed closely by a face centered cubic (fcc) and a hexagonal close packed (hcp). These different structures have very small fractional difference of Coulomb energies per ion, typically $< 10^{-4}$. Numerical simulations using a planar model[7] suggest that one need at least 60 inter-particle spacings to observe bulk behavior; that is $N > 10^5$ ions are necessary in a spherical plasma to exhibit bulk properties. More recently numerical simulations of spherical plasma[8] have suggested that a bcc lattice may be present in small sections of a plasma with as little as 15,000 ions.

The inner particles spacing of Coulomb crystals is $\sim 10\mu$m, therefore Bragg scattering can be performed on them with ultraviolet light instead of x-ray as for solid state crystals. Since Coulomb crystals contain only a small number of ion compared to solid state crystals, the wavelength is chosen to be resonant with an atomic transition to increase the scattering cross-section.

Figure 3 shows the NIST trap designed to study large coulomb crystals.

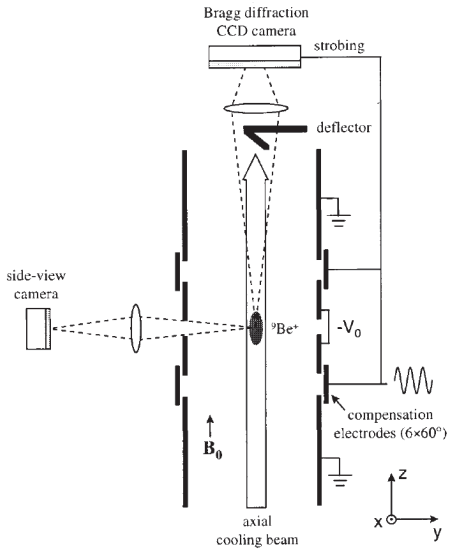

Fig. 3. NIST Cylindrical Penning trap for large crystal.

The inside diameter of the trap is 4.5cm and the magnetic field $B = 4.5$T. In this trap Beryllium ions can be laser cooled down to $T < 1$mK. The Bragg scattering is done by an axial beam. The direct beam is deflected to avoid saturating the CCD camera, and crossed polarizers are used to further minimize unwanted scattering from the entrance window.[9]

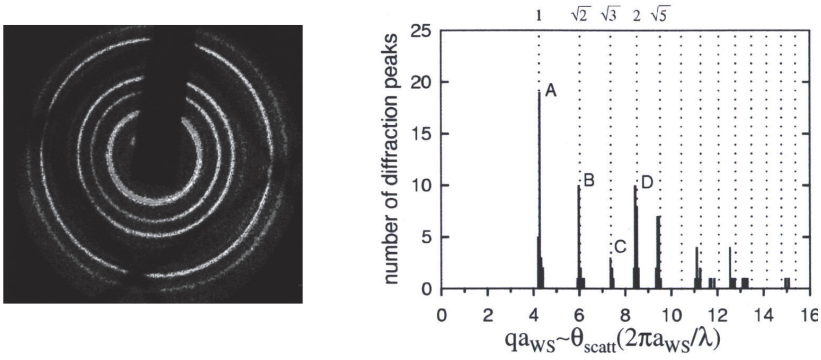

Fig. 4. Bragg scattering rings and frequency of ring location.

Scattering pictures are shown on figure 4. The location of scattering rings indicates that the Coulomb crystal structure is bcc. Since the scattering picture are accumulated over several plasma rotations, it is not possible to distinguish a single crystal from several smaller crystals in the trap. Similarly x-ray diffraction on powdered crystal result in diffraction rings. Locking the crystal rotation to the rotating wall and strobing the camera at the rotating wall frequency determines unambiguously that a single crystal is in the trap. Figure 7 in the chapter describing the rotating wall technique shows a strobed diffraction pattern corresponding to a bcc crystal.

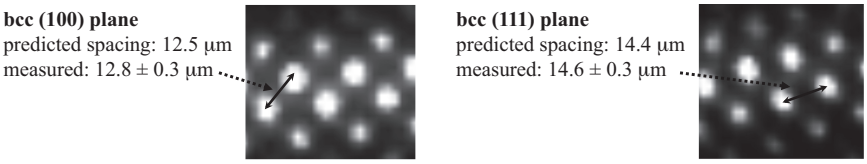

Fig. 5. Real space images of bcc coulomb crystal.

Real space images of the plasma also confirm a bcc crystal. Depending on the orientation of the probe laser beam the (100) plane or the (111)

plane can be illuminated as shown on figure 5. The spacing of the ions in the (100) plane and the (111) plane are in agreement with a bcc crystal.

Summary of Correlation on Equilibrium Properties

For plasmas with $N < 10^4$ ions, the boundary effects dominate and shell structure is observed. For large plasmas, with $N > 10^5$ ions, bcc Coulomb crystals are observed in spheroidal plasma.

3. Effect of Correlations on a Dynamical property

In this section, we will briefly describe theory results and measurements that use non-neutral plasmas to model aspects of the physics of nuclear fusion reactions in dense, correlated plasmas, such as in giant planets, degenerate stars, and laser fusion plasmas. Nuclear reaction rates in dense correlated plasmas are, according to theory, enhanced compared to rates predicted for reactions at lower density. In the astrophysics community, this theoretical effect is known as the Salpeter enhancement.[10] Here we use an analogy between screened nuclear reactions in dense plasmas and perpendicular-to-parallel energy equipartition in strongly coupled and strongly magnetized non-neutral plasmas.[11,12]

In a magnetized plasma (i.e. $\Omega_c \gg \omega_p$) with a perpendicular temperature $T_\perp$ and a parallel temperature $T_\parallel$, we consider the perpendicular-to-parallel collision rate $\nu_{\perp\parallel}$ defined as:

$$\frac{d}{dt}T_\perp = \nu_{\perp\parallel}\,(T_\parallel - T_\perp) \tag{17}$$

with

$$\nu_{\perp\parallel} \equiv n\bar{v}b^2\; 4\sqrt{2}I(\bar{\kappa})\; g(\Gamma) \tag{18}$$

Here the "bare" collision rate $4\sqrt{2}\; n\bar{v}b^2$ is modified by a dynamical factor $I(\bar{\kappa})$ depending only on the magnetization parameter

$$\bar{\kappa} \equiv \sqrt{2}\;\frac{b}{r_c} \tag{19}$$

and modified by an correlation factor $g(\Gamma)$, depending only on the correlation parameter Γ. Where b is the distance of closest approach

$$b \equiv \frac{e^2}{4\pi\epsilon_0 a_{ws} k_B T} \tag{20}$$

$I(\bar{\kappa})$ suppress the perpendicular to parallel collision in the strongly magnetized regime of $\bar{\kappa} > 1$. In this regime only rare energetic collisions mix the perpendicular energy $E_\perp$ and parallel energy $E_\parallel$.

The correlation factor $g(\Gamma)$ enhances these rare collisions due to particle correlations, in the cryogenic liquid regime of $1 < \Gamma < 10$.

3.1. *Strong Magnetization*

I will briefly review the strong magnetization regime results, a rigorous derivation can be found in reference 11. For $r_c < b$, the perpendicular energy of two particles is an adiabatic invariant $E_\perp = E_{\perp 1} + E_{\perp 2}$, that is conserved by most collisions except by rare energetic (large $E_\parallel$) collision. The cross-section for sharing perpendicular and parallel energy is a function of $E_\parallel$:

$$\sigma(E_\parallel) \propto \exp\left[-\pi\left(\frac{b}{r_c}\right)\right] \approx \exp\left[-\pi\left(\frac{Cst}{E_\parallel}\right)^{\frac{3}{2}}\right] \tag{21}$$

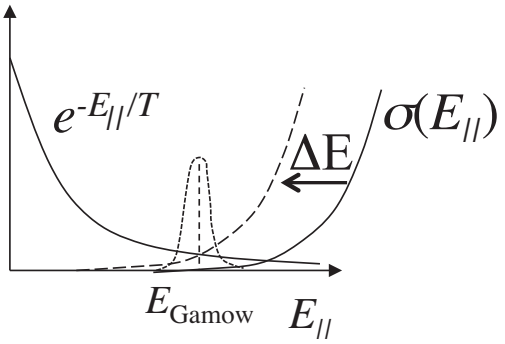

Fig. 6. Graphic description of the integrand of equation 22 showing exponentially decaying Maxwellian particle energy distribution and the exponentially growing cross-section σ. The product of the particle distribution and the cross-section gives rise to the Gamow peak. Shifting σ by ΔE gives enhancement $\exp(\Delta E/k_B T)$.

That is the cross-section for $E_\parallel - E_\perp$ sharing increases exponentially for large $E_\parallel$. The collision rate is obtained by integrating the product of the maxwellian particles distribution and $\sigma(E_\parallel)$.

$$\nu_{\perp\parallel}^{\text{no corr}} = \int dE_\parallel \; \frac{1}{k_B T} \; \exp\left(-\frac{E_\parallel}{k_B T}\right) \sigma(E_\parallel) = n\bar{v}b^2 4\sqrt{2}\, I(\bar{\kappa}) \tag{22}$$

where $I(\bar{\kappa})$ is:[13]

$$I(\bar{\kappa}) \approx 1.5 \exp\left(-2.044\ \bar{\kappa}^{\frac{2}{5}}\right) \tag{23}$$

The Maxwellian has almost no particles at large $E_\parallel$ and the cross-section is large at large $E_\parallel$ as shown on figure 6. Most of the collisions causing sharing of $E_\parallel$ and $E_\perp$ comes from the "Gamow" peak shown on figure 6. For example for $\bar{\kappa} = 20$ the Gamow peak is located at $4\bar{v}$ that is less than 2% of the particles participate in such "rare" collision. The cyclotron energy is released only by rare collision, analog to fusion reaction where the energy stored in the nuclei is liberated only by rare energetic collision.

3.2. *Correlations*

Correlations enhance the perpendicular-to-parallel collision rate through screening effects, by reducing the amount of parallel energy required by two ions to come within a distance ρ. In the absence of shielding the energy required is:

$$E_\parallel = \frac{e^2}{4\pi\epsilon_0\rho} \tag{24}$$

in contrast, with Debye screening the parallel energy required is smaller:

$$E_\parallel = \frac{e^2}{4\pi\epsilon_0\rho} \exp\left(\frac{-\rho}{\lambda_D}\right) \simeq \frac{1}{4\pi\epsilon_0}\left[\frac{e^2}{\rho} - \frac{e^2}{\lambda_D}\right] \tag{25}$$

In other words, screening reduces the parallel energy required to come within a distance ρ. In the strong coupling regime of $\Gamma > 1$, the effective shielding distance is the inter-particle spacing, and the energy required for a collision at distance $\rho < a_{ws}$ is:

$$E_\parallel \simeq \frac{1}{4\pi\epsilon_0}\left[\frac{e^2}{\rho} - \frac{e^2}{a_{ws}}\right] \tag{26}$$

This shift the cross-section $\sigma(E_\parallel)$ by $\Delta E_\parallel = e^2/(4\pi\epsilon_0 a_{ws})$ as shown in figure 6. Equivalently, the Maxwellian in equation 22 is shifted by $\Delta E_\parallel/(k_B T)$ $= e^2/(4\pi\epsilon_0 a_{ws} k_B T) = \Gamma$, therefore equation 22 becomes:

$$\begin{aligned}
\nu_{\perp\parallel}^{corr} &\simeq \int dE_\parallel\ \frac{1}{k_B T}\ \exp\left(-\frac{E_\parallel}{k_B T} - \frac{e^2}{4\pi\epsilon_0 a_{ws} k_B T}\right)\sigma(E_\parallel) \\
&= \exp\left(\frac{e^2}{4\pi\epsilon_0 a_{ws} k_B T}\right)\int dE_\parallel\ \frac{1}{k_B T}\ \exp\left(-\frac{E_\parallel}{k_B T}\right)\sigma(E_\parallel) \\
&= \exp(\Gamma)\ \ \nu_{\perp\parallel}^{no\ corr}
\end{aligned} \tag{27}$$

Correlation increases the perpendicular to parallel collision rate by a factor of roughly $g(\Gamma) = \exp(\Gamma)$. It is worth noting that the enhancement is independent of $\sigma(E)$, as in the fusion case, where this effect is known as the Salpeter enhancement.

3.3. *Experiments*

To test the theoretically predicted correlation enhancement of the collision rate, we use a magnesium ion plasma contained in a Penning-Malmberg trap. The plasma density for this experiment is controlled with a rotating wall ($0.12 \times 10^7 \leq n \leq 2 \times 10^7 \mathrm{cm}^{-3}$), the temperature ($2.5 \times 10^{-6} \leq T \leq 1\mathrm{eV}$) is controlled by laser cooling, the uniform axial magnetic field was changed in the range of $1.2\mathrm{T} \leq B \leq 3\mathrm{T}$. The adiabaticity parameter $\bar{\kappa}$ is equal to one at a temperature $T = 5 \times 10^{-4}\mathrm{eV}$ and B=3T. The coupling parameter is $\Gamma = 1$ for $n = 2 \times 10^7 \mathrm{cm}^{-3}$. and $T = 6 \times 10^{-5}\mathrm{eV}$.

The measured perpendicular-to-parallel collision rate is plotted in figure 7 for two densities $n = 2 \times 10^7$ and $0.12 \times 10^7 \mathrm{cm}^{-3}$ labeled $n_7 = 2$ and $n_7 = 0.12$ In both cases the collision rate is strongly suppressed when $\bar{\kappa}$ is larger than unity. The solid lines are theory curves obtained from equation 22 using numerical values of $I(\bar{\kappa})$ from reference[13] with no adjustable parameters.

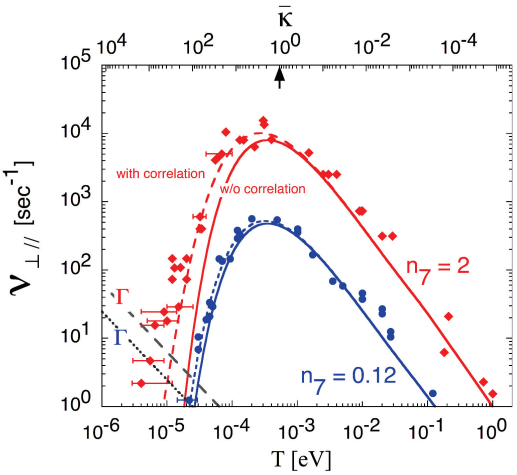

Fig. 7. Measured collision rates for two densities versus temperature (lower axis) and $\bar{\kappa}$ (upper axis) compared to theory with and without correlations. The correlation parameter Γ for high and low density is also shown.

The dashed lines are from equation 27. At lower density the plasma is never strongly correlated, as shown by Γ which is also plotted for both densities. The $n = 2 \times 10^7$ cm^{-3} density labeled $n_7 = 2$ has $\Gamma > 1$ at low temperatures, and the measured collisionality is enhanced by several orders of magnitude over theory neglecting correlations. At low density, the collision rate is measured down to a rate of 1 sec^{-1}, setting an upper limit on extraneous collisional effects. Figure 8 shows the measured collision rate divided by the theoretical rate neglecting correlations, that is, the Salpeter enhancement $g(\Gamma)$. The enhancement depends on Γ but is independent of $\bar{\kappa}$, as predicted by theory. The measured correlation enhancement $g(\Gamma)$ is consistent with equilibrium shielding theories, and no support for alternative dynamic shielding effects is seen.

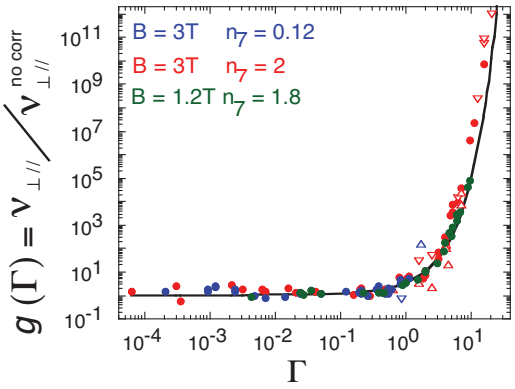

Fig. 8. Correlation enhancement $g(\Gamma)$ of the collision rate versus the correlation parameter Γ.

This work illustrates how laboratory non-neutral plasmas can be used to study high energy density plasmas where the same enhancement applies to rare energetic fusion collisions in hot, dense correlated plasmas such as stars.

Summary of Perpendicular to Parallel Collision Rate

Perpendicular to parallel collision rate are strongly suppressed in the "strong magnetization" regime of $\bar{\kappa} > 1$. Only rare energetic collisions cause $E_\perp$ to $E_\parallel$ energy exchange. These rare energetic collisions are strongly enhanced in the correlated liquid and crystal regime. Enhancement of up to 10^9 over uncorrelated theory are observed. The same enhancement applies

to rare energetic fusion collisions in hot, dense, correlated plasmas such as stars.

4. Tutorial Problem

Devise a technique to measure the perpendicular to parallel collision rate $\nu_{\perp\parallel}$ in a magnetized plasma. Hint: look at equation 17 to see which physical quantities have to be perturbed to measure the collision rate $\nu_{\perp\parallel}$.

A detailed description of two different techniques is given in reference 12. The first technique directly observes $T_\perp$ and $T_\parallel$ as they relax to a common temperature. The parallel temperature is initially increased by small oscillating voltages applied at one end of the plasma. This direct measurement is practical only for slow rates ($\nu_{\perp\parallel} < 100\text{sec}^{-1}$) due to photon counting rate limitations, and is not accurate for low temperatures ($T < 10^{-4}\text{eV}$) since ion-neutral collisions give a heating rate which dominates the temperature evolution.

The second technique also uses small oscillating voltages applied at one end of the plasma. This acts as a piston and alternatively compress and expand the plasma in the axial direction. If the oscillation frequency f_{osc} is large compared to the collision rate, the cycle is a reversible process since heat is not transfer to the perpendicular degrees of freedom. Similarly, if the oscillation frequency is slow compare to the collision rate, the cycle is also reversible, since heat is fully shared with the perpendicular degrees of freedom. In contrast if $f_{osc} \sim \nu_{\perp\parallel}$, the process is not reversible: more work is done during the compression stroke and the excess appears as plasma heat. The maximum heat per cycle occurs when $2\pi f_{osc} C \simeq \nu_{\perp\parallel}$ where C is the specific heat at constant density of a magnetized plasma. In the absence of correlations $C = 1/3$; and C increases slightly in the presence of correlations.

Acknowledgements

This work was supported by National Science Foundation Grant PHY-1414570, Department of Energy Grant DE-SC0002451and Department of Energy High Energy Density Laboratory Plasma Grant DE-SC0008693. The author thanks the organizers of Les Houches Winter School for the opportunity to contribute to the workshop. The author also thanks Prof. C.F. Driscoll, Prof. D.H.E. Dubin and Prof. T.M.O'Neil for many years of

enlightening guidance and theoretical support.

References

1. Frontiers in High Energy Density Physics, NRC, The National Academies Press, Washington, DC (2003).
2. V.E. Fortov, A.G. Khrapak, S.A. Khrapak, V.I. Molotkov, O.F. Petrov, Dusty plasmas, *Physics-Uspekhi*, **47**, 447-492, (2004). H. Thomas, G. Morfill, V. Demmel, J. Goree, B. Feuerbacher, and D. Mhlmann, Plasma Crystal: Coulomb Crystallization in a Dusty Plasma, *Physical Review Letters* **72**, 652-656, (1994).
3. D.H.E. Dubin and T.M. O'Neil, Trapped Nonneutral Plasmas, Liquids, and Crystals (The Thermal Equilibrium States), *Rev. Mod. Phys.* **71**, 87-172, (1999). T.M. O'Neil and D.H.E. Dubin, Thermal Equilibria and Thermodynamics of Trapped Plasmas with a Single Sign of Charge, *Phys. Plasmas* **5**, 2163-2193, (1998).
4. S.G. Kuzmin and T.M. O'Neil, Numerical Simulation of Ultracold Plasmas, *Phys. Plasmas* **9**, 3743 (2002).
5. D.H.E. Dubin and T.M. O'Neil, Computer Simulation of Ion Clouds in a Penning Trap, *Phys. Rev. Lett.* **60**, 511 (1988). D.H.E. Dubin, Effect of Correlations on the Thermal Equilibrium and Normal Modes of a Nonneutral Plasma, *Phys. Rev. E* **53**, 5268 (1996).
6. S.L. Gilbert, J.J. Bollinger, and D.J. Wineland, Shell-Structure Phase of Magnetically Confined Strongly Coupled Plasmas, *Phys. Rev. Lett.* **60**, 2022-2025 (1988).
7. D.H.E. Dubin, Correlation Energies of Simple Bounded Coulomb Lattices, *Phys. Rev. A* **40**, 1140 (1989).
8. Hiroo Totsuji, Tokunari Kishimoto, Chieko Totsuji, and Kenji Tsuruta, Competition between Two Forms of Ordering in Finite Coulomb Clusters, *Phys. Rev. Lett.* **88**, 125002, (2002).
9. W.M. Itano, J.J. Bollinger, J.N. Tan, B. Jelenkovic, X.-P. Huang, and D.J. Wineland, Bragg diffraction from crystallized ion plasmas, *Science* **279**, 686-689 (1998).
10. E. E. Salpeter, Electron Screening and Thermonuclear Reactions, *Aust. J. Phys.* **7** , 373 (1954); E. E. Salpeter and H. Van Horn, Nuclear Reaction Rates at High Densities, *Astrophys. J.*, **155**, 916 (1969).
11. D.H.E. Dubin, Modeling Nuclear Fusion in Dense Plasmas Using a Cryogenic Non-neutral Plasma, *Phys. Plasmas* **15**, 055705 (2008).
12. F. Anderegg, D. H. E. Dubin, T. M. O'Neil and C. F. Driscoll, Measurement of Correlation-Enhanced Collision Rates, *Phys. Rev. Lett.* **102**, 185001 (2009).
13. M.E. Glinsky, T.M. O'Neil, M.N. Rosenbluth, K. Tsuruta and S. Ichimaru, Collisional Equipartition Rate for a Magnetized Pure Electron Plasma, *Phys. Fluids B* **4**, 1156 (1992).